

## Article

# The Geology, Petrography, and Geochemistry of Egyptian Dokhan Volcanics: A Potential Source for Construction Aggregate

Hatem El-Desoky<sup>1</sup>, Nabil Abd El-Hafez<sup>1</sup>, Ahmed Khalil<sup>2</sup>, Ahmed Arafat<sup>3,\*</sup>, Mahmoud Galal Hasan<sup>4</sup> and Tarik Youssef<sup>5,\*</sup>

<sup>1</sup> Department of Geology, Faculty of Science, Al-Azhar University, Cairo 11651, Egypt

<sup>2</sup> Department of Geology, National Research Center, Dokki, Cairo 12622, Egypt

<sup>3</sup> Faculty of Science, Al-Azhar University, Cairo 11651, Egypt

<sup>4</sup> Structural Engineering Department, Ain Shams University, Cairo 11566, Egypt

<sup>5</sup> Faculty of Engineering, L'Universite Française D'Egypte, Alshorouk City, Cairo 11837, Egypt

\* Correspondence: arafatahmed048@gmail.com (A.A.); tarik.youssef@ufe.edu.eg (T.Y.)

**Abstract:** The present paper focuses on the geology, petrography, and geochemistry of the well-known Dokhan volcanics encountered in the northern part of the Eastern Desert of Egypt. The basalts, andesites, rhyolites, and agglomerates exposed at the Makhar Seal (flood plain) as well as Wadi Abu Zoghot, Wadi El-Ghafiryia, Wadi Al-Radah Luman, Wadi Al-Ushsh, Wadi Umm Sidrah, and Gabal Ghuwayrib are herein examined as sources of coarse aggregate in concrete mixes. A representative total of 28 samples—collected from different Dokhan volcanics—was studied in terms of field geology, petrography, and geochemistry wherein a variety of experiments related to construction material validation apply. The petrographic examination revealed that the studied Dokhan volcanics consist of basic, intermediate, and acidic volcanic igneous rocks. These rocks are represented through basalts, andesites, imperial porphyry, dacites, rhyodacites, rhyolites, and their pyroclastics. Furthermore, the applied geochemical analysis indicated that the studied Dokhan volcanics are alkaline to sub-alkaline, calc-alkaline and classified as basalts, basaltic andesites, andesites, trachyandesites, trachydacites, trachytes, and rhyolites, indicating an initial potential as aggregate for concrete mixes. Finally, the results obtained from incorporating Dokhan volcanics as aggregates in concrete mixes demonstrated a significant improvement in regard to the properties of the comprising concrete mixes. Herein, a higher compressive strength was witnessed after 28 days for Dokhan volcanic concrete, when compared to concrete comprising dolomite aggregate, amounting to an average increase that exceeded 36%.

**Keywords:** Dokhan volcanics; petrography; geochemistry; coarse aggregate; concrete mixes



**Citation:** El-Desoky, H.; Abd El-Hafez, N.; Khalil, A.; Arafat, A.; Hasan, M.G.; Youssef, T. The Geology, Petrography, and Geochemistry of Egyptian Dokhan Volcanics: A Potential Source for Construction Aggregate. *Minerals* **2023**, *13*, 635. <https://doi.org/10.3390/min13050635>

Academic Editors: Vasilios Melfos, Panagiotis Voudouris and Grigorios Aarne Sakellaris

Received: 28 January 2023

Revised: 26 April 2023

Accepted: 27 April 2023

Published: 2 May 2023



**Copyright:** © 2023 by the authors. Licensee MDPI, Basel, Switzerland. This article is an open access article distributed under the terms and conditions of the Creative Commons Attribution (CC BY) license (<https://creativecommons.org/licenses/by/4.0/>).

## 1. Introduction

Concrete is indeed the most important material in the construction industry. It comprises water, cement, fine aggregate, and coarse aggregate. The latter component typically consists of crushed rock that forms up to 60–80% of the concrete volume and 70–85% of the concrete mass. The presence of coarse aggregate is paramount for the strength, thermal, and elastic properties of concrete, as well as concrete dimensional and volume stability. For the last two decades, the number of ready-mix concrete batch plants worldwide has increased exponentially.

In Egypt, more than 50 million cubic meters of concrete were produced in 2021; dolomitic rocks represent around 75–85% of concrete aggregates, produced mostly from the quarries of Gabal Ataqa (located between the Suez Governorate and the Red Sea Governorate). However, recently, ongoing developments within Gabal Ataqa to transform it into a tourist attraction have ended up closing many existing quarries. The most popular

of such aggregate-producing sites are namely Ben Laden, El-Daly, New-Gravel, Ready-Rocks, El-Khawaja and Lafarge. In turn, exploring and discovering aggregate substitutes has become a necessity.

Several authors have studied alternatives to dolomitic aggregates: e.g., Ismail and Ghabrial [1] studied the use of acidic igneous rocks (granites) as aggregate in concrete production; ref. [2] studied the use of basic Dokhan volcanics as aggregate in concrete mixes; and ref. [3] presented a study exploring the feasibility of basalt aggregates in concrete mixtures. The latter also used normal laboratory tests and slump test analysis along with calculating the compressive strength of the mixture. In ref. [4], the effect of incorporating volcanic tuff into cement mortar was investigated. The outcome demonstrated a significant enhancement in flexural strength. Ref. [5] investigated the geological properties of Azorean lava rocks as regarded their alkali and silica content; adverse effects on the properties of building materials were observed. The application of advanced computing and optimization methods onto volcanic rocks to compute compressive strength was evident in [6]. In ref. [7], a comparative analysis was conducted on the eligibility of volcanic rocks within concrete mixtures, in terms of workability, compressive strength, and bulk density. The researchers of [8] investigated the potential effect of volcanic rock aggregates when mixed with concrete materials to ameliorate their compressive and tensile strength(s). Refs. [9,10] carried out a study to investigate the effect of rocks from volcanic sites on the industrial utilities of Turkey and Bologna (Italy). The effort at hand infers upon the geology, petrography, and geochemistry of Dokhan volcanics in Egypt and the possibility of their utilization as aggregates in concrete mixes. For this purpose, six field occurrences of Dokhan volcanics were investigated: Makhar Seal Wadi Abu Zoghot, Wadi El-Ghafiryia, Wadi Al-Radah–Luman, Wadi Al-Ushsh, Wadi Umm Sidrah, and Gabal Ghuwayrib (along El-Sokhna–Hurghada Road) (Figure 1).

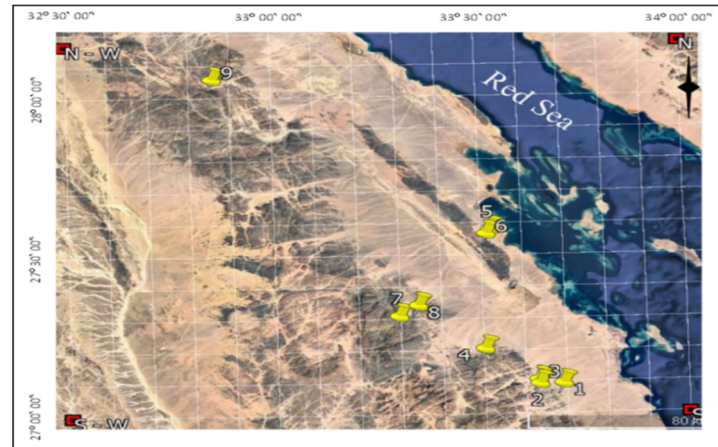


**Figure 1.** Landsat image showing the location of the studied Dokhan volcanics regions encountered in Egypt. 1. Makhar Seal Wadi Abu Zoghot. 2. Wadi Al-Radah Luman. 3. Wadi Al-Radah Luman. 4. Wadi El-Ghafiryia. 5. Wadi Al-Ushsh. 6. Wadi Al-Ushsh (Wadi Mleiha). 7. Wadi Umm Sidrah. 8. Wadi Umm Sidrah. 9. Gabal Ghuwayrib.

## 2. Materials and Methods

Eighteen Dokhan volcanics samples were collected from the studied area (the northern part of the Eastern Desert of Egypt), then crushed, and powdered using a stainless steel jaw crusher and an agate ball mill machine. This was performed at the laboratories of the National Research Center of Egypt (NRC). Accordingly, (i) petrography and (ii) geochemical characteristics were identified. The chemical composition of major oxides and trace elements was determined for the studied Dokhan volcanic samples by using an X-ray fluorescence spectrometer (Model A: Philips Pw/2404, 30 kV), available at the Housing and Building National Research Center (HBRC), Cairo, Egypt. Standard petrographic thin sections were prepared and examined to analyze the microfabrics, identify the Dokhan

volcanics' minerals, their mineralogical composition, as well as their structure and texture. Concrete samples comprising crushed volcanics as aggregate were prepared according to the Egyptian standards No. 1658 (1991), Part five, "Method for Casting Test Cubes", as well as the British Standards (BS) 1881-Part 108-1983 and ASTM C-192 (1988), "Method for Making Test Cubes from Fresh Concrete". The BS EN 12350-2 (2000), "Testing Fresh Concrete D Part 2: Slump test", was also considered, where mixing a specified weight of aggregate, sand, cement, and water was conducted as follows: The studied samples were cast within a 150 mm × 150 mm × 150 mm mold, consequently samples were compacted using a standard compaction rod of 1.8 Kg mass, 380 mm long, and of a 25 mm squared cross-section. The samples were cured in a treatment unit comprising heaters and air conditioning to maintain a temperature within the standard limits of  $21 \pm 3$  °C. The samples were tested using a calibrated and certified 1500 kN compression testing machine.

### 3. Geological Setting

The Dokhan volcanics under investigation are classified into basic (basalts), intermediate (andesites), and acidic (rhyolites) igneous rocks. They are composed of a series of volcanic rocks ranging from basalts to andesites and rhyolites, formed towards the end of the Precambrian era in the Egyptian basement complex, where the best type of locality is recognized as the Gabal Dokhan region in the northern part of the Eastern Desert. Dokhan volcanics have been studied by several authors [11–22].

Dokhan volcanics occupy a vast area, forming moderately high mountainous ridges. They consist of varicolored alternating successions of lava flows of basic, intermediate, and acidic composition, interlayered with pyroclastic rocks. Repeated eruptions of the volcanic materials have locally produced layered structures as shown in Figure 2.

The basic Dokhan volcanics are characterized by dark gray to black and blackish green colors (Figure 3). Herein, basaltic rocks appear as rock extrusions within the granitic rocks encountered in the Makhar Seal Wadi Abu Zoghot, whereas syenogranites serve as intrusions within the basaltic rocks exposed at Wadi El-Ghafiryia. Basic and intermediate Dokhan volcanics extruded within Al-Ushsh monzogranites are evident. Andesites, basalts with dacites' variety of porphyritic and flow textures, are developed along with laminated lapilli tuffs and agglomerates exposed at Gabal Ghuwayrib and Wadi Al-Radah–Luman. Tholeiitic basalts encountered are associated with the intermediate and pyroclastic rocks and many felsic dykes extruded within Umm Sidrah Dokhan volcanics. The intermediate Dokhan volcanics demonstrate the presence of andesites and quartz andesites. The studied intermediate Dokhan volcanics, represented by andesite porphyry exposed at Wadi Al-Radah-Luman, are exhibited as massive, jointed, and fractured layers of a light gray color. Wadi Al-Ushsh andesitic rocks are extruded into monzogranites, whereas pyroxene andesites and biotite quartz trachytes, associated with basic Dokhan volcanics, are encountered in Wadi Umm Sidrah and Gabal Ghuwayrib. Basic and intermediate Dokhan volcanics are extruded within Wadi Al-Ushsh monzogranites. Acidic Dokhan volcanics are represented by spherulitic rhyolites, associated with basic and intermediate volcanics at Gabal Ghuwayrib, also exhibiting buff rhyolites. Dokhan volcanics are jointed, fractured, and light gray in color at Wadi Al-Radah-Luman. Pyroclastics are the individual crystals, crystal fragments, glass, and rock fragments generated by disruption, as a direct result of volcanic action [23]. Pyroclastics are produced from the consolidation of pyroclastic accumulations into a coherent rock type and take many names such as ash tuff, lapilli tuff, tuff breccia, pyroclastic breccia, and agglomerate. The studied agglomerate is exposed at Umm Sidrah and Gabal Ghuwayrib, associated with basic and intermediate Dokhan volcanics (Figure 3).

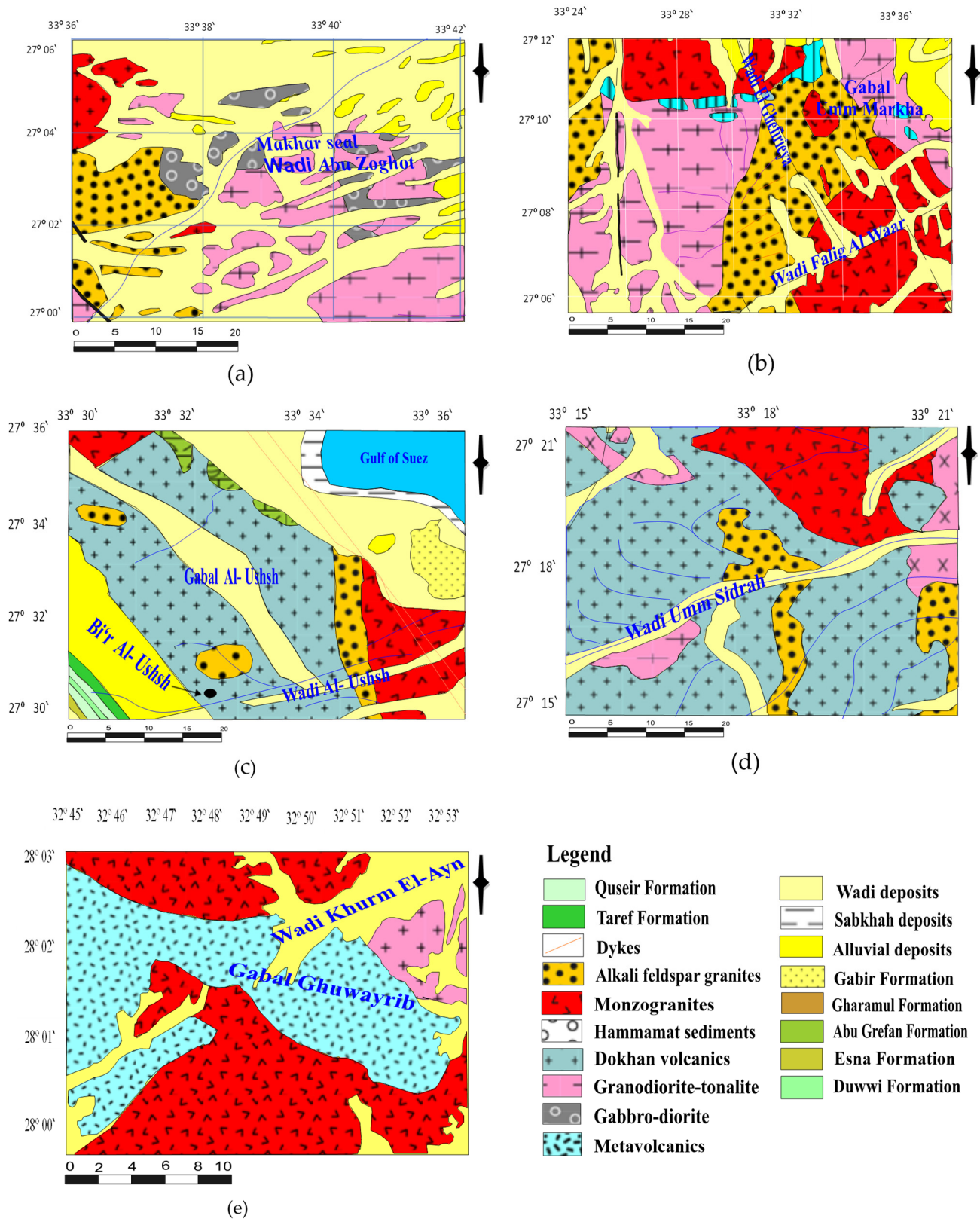
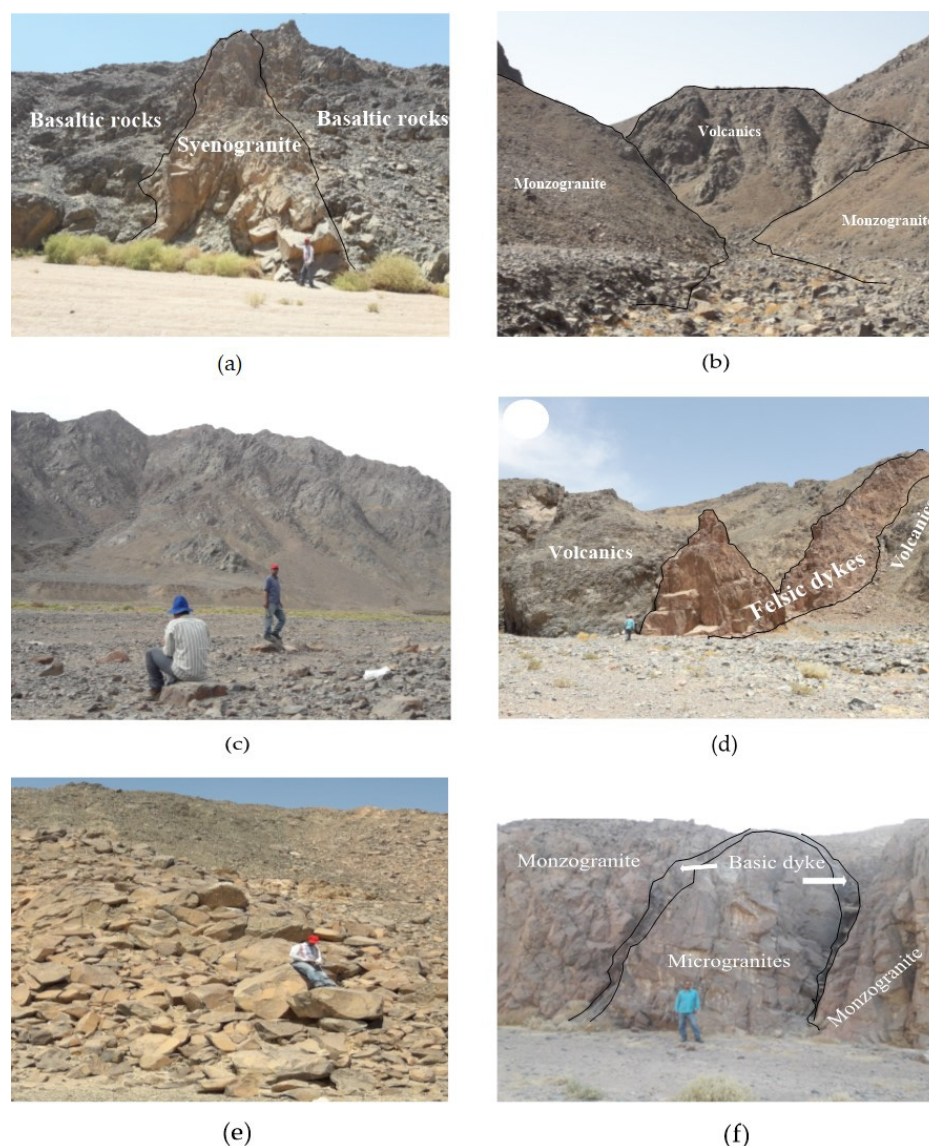


Figure 2. (a–e) Geological maps of the study regions [24].



**Figure 3.** (a–f) Photographs showing the following geological features: (a) syenogranites were intruded by basaltic rocks at Wadi El-Ghafiryia (looking N–W); (b) Dokhan volcanics (basic and intermediate) extruded within Al-Ushsh monzogranites (looking E–W); (c) Dokhan volcanic andesite, basalts with dacites' variety of porphyritic texture, laminated lapilli tuffs, and agglomerates (looking N–W); (d) tholeiitic basalts extruded by felsic dykes of Dokhan volcanics at Wadi Umm Sidrah (looking E–W); (e) rhyolite appears massive, jointed, fractured, and light gray in color as shown in Wadi Al-Radah–Luman (looking N–W); and (f) basic and intermediate Dokhan volcanics are extruded within Al-Ushsh monzogranites.

## 4. Results

### 4.1. Petrography

The Dokhan volcanics under study are represented by trachybasalts, tholeiitic basalts, andesites, spherulitic rhyolites, and their pyroclastics. Trachybasalts consist mainly of plagioclase, pyroxene (titanaugite), and hornblende as well as some accessory minerals such as biotite and opaques. Secondary minerals are represented by saussurite, quartz, and carbonate minerals (calcite). Plagioclase occurs as medium- to fine-grained, tabular prismatic crystals which are partially altered to saussurite, set in a fine-grained groundmass from plagioclase, with a trachytic texture. Pyroxene (titanaugite) occurs as euhedral prismatic crystals of yellowish green and dark green colors, medium- to coarse-grained set in fine-grained groundmass, from plagioclase partially altered to pyroxene titanaugite. Horn-

blende occurs as subhedral prismatic crystals demonstrating two sets of cleavage, subhedral crystals set in fine-grained groundmass, occasionally altered to chlorite. Opaque minerals occur as dispersed grains between other mineral constituents. Finally, saussurite occurs as fine to medium grains as a result of plagioclase totally altered to epidote. Tholeiitic basalts consist of plagioclase and pyroxene (pigeonite-hypersthene) as essential minerals in addition to accessory minerals such as biotite and opaque minerals. Secondary minerals such as saussurite, chlorite, and iron oxides are also present. Plagioclase occurs as medium- to coarse-grained, partially to totally altering to saussurite. Pyroxene (pigeonite-hypersthene) occurs as medium- to coarse-grained, set-in fine-grained groundmass from plagioclase, biotite, and opaque minerals. Biotite occurs with iron oxides in clots. Saussurite minerals occur in fine grains of allanite, zoisite, and epidote, as a result of totally altered plagioclase and biotite altered to chlorite (Figure 4).

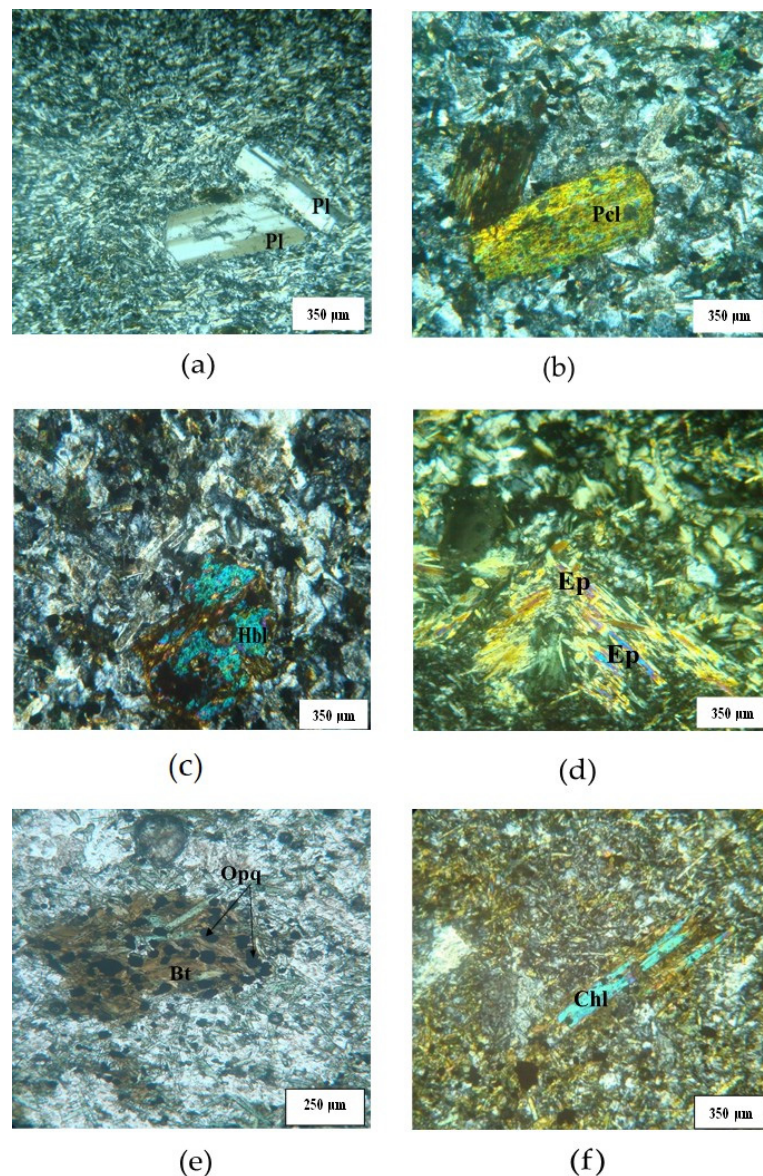


**Figure 4.** (a–f) Photomicrographs showing the main petrographic features of basic Dokhan volcanics. Mineral abbreviations were taken from [25]. (a) Tabular prismatic plagioclase crystals exhibit a porphyritic texture (CN). (b) Pyroxene partially altered to chlorite (CN). (c) Hornblende phenocrysts occur as subhedral crystals (CN). (d) Plagioclase occurs as fine-grained totally altered to epidote (CN). (e) Pyroxene altered to chlorite and iron oxides (PPL). (f) Biotite altered to chlorite (CN).

The common intermediate Dokhan volcanics comprise andesites that are fine- to medium-grained and range from aphanitic to typical porphyritic varieties. They consist of plagioclase, pyroxene (titanaugite), hornblende, and quartz as essential minerals. The accessory minerals consist of biotite, tremolite-ferroactinolite, titanite, apatite, and opaques. Meanwhile chlorite, calcite, and saussurite occur as secondary minerals. Plagioclase occurs as medium- to coarse-grained, tabular prismatic crystals that exhibit Carlsbad twinning set in glassy groundmass, partially altered to saussurite minerals. Occasionally, plagioclase occurs as medium to coarse grains of a glomeroporphyritic texture. On the other hand, pyroxene and hornblende occur as medium- to coarse-grained anhedral crystals, having one or two cleavages. These crystals are interbedded with ophitic to subophitic textured pyroxene, partially altered to chlorite. Quartz occurs as essential minerals due to the complete growth of crystals (subhedral and anhedral phenocrysts) that are scattered in fine-grained groundmass. The latter occurs as secondary minerals that fill the vugs in other cases. Biotite, chlorite, and opaques occur together in clots; biotite occurs as fine to medium grains (subhedral to anhedral crystals), partially altered to chlorite wherein biotite and quartz grains take a trill-like shape. Titanite occurs as brown or yellowish brown fine grains scattered between the other minerals, often not visible in hand specimens, and is usually associated with iron oxide, hornblende, and plagioclase, adopting a sphenoidal shape. Finally, apatite occurs in short, minute, needle shapes and colorless crystals associated with felsic constituents (Figure 5).

Acidic Dokhan volcanics, represented by spherulitic rhyolites, are composed essentially of phenocrysts of quartz, plagioclase, and orthoclase, as well as other accessory mineral scattered flakes of biotite and sericite. Chlorite and epidote are present as secondary minerals. A spherulitic texture emerges as a result of the substitution of plagioclase by K-feldspar. Spherulite consists of a dense mass of very fine intergrown needles of both quartz and feldspar that radiate from a common nucleus. Both spherulitic and porphyritic textures are recognized in the studied spherulitic rhyolites. Plagioclase occurs as few deformed prismatic phenocrysts, euhedral, and small subhedral crystals. Orthoclase occurs as irregular euhedral crystals, characterized by shadow extinction that is highly cloudy due to the alteration of kaolinite and sericite. Biotite occurs as accessory brownish minerals and pale brownish anhedral pleochroic flakes, associated with sericite crystals, partly or highly altered to chloritized biotite and chlorite. Finally, chlorite occurs as secondary minerals comprising pale green flakes, and subhedral to anhedral crystals (Figure 6).

As regards the existing pyroclastic Dokhan volcanics in this effort, they are represented by agglomerates having the same mineral composition. Anhedral to subhedral quartz, plagioclase, biotite, devitrified glass, and opaques are recognized as the main mineral phases of phenocrysts (relic) as well as in reconstituted groundmass. Plagioclase occurs as medium to coarse grains, tabular prismatic crystals exhibiting Carlsbad twinning, set in fine- to medium-grained groundmass, partially altered to epidote. Quartz occurs as subhedral and anhedral phenocrysts that are scattered in fine-grained groundmass. Biotite occurs as accessory minerals, brownish and pale brownish in color, accompanied with opaques in clots, and partially altered to chlorite. Carbonate (calcite) occurs as secondary minerals that fill microfractures and vugs (Figure 7).

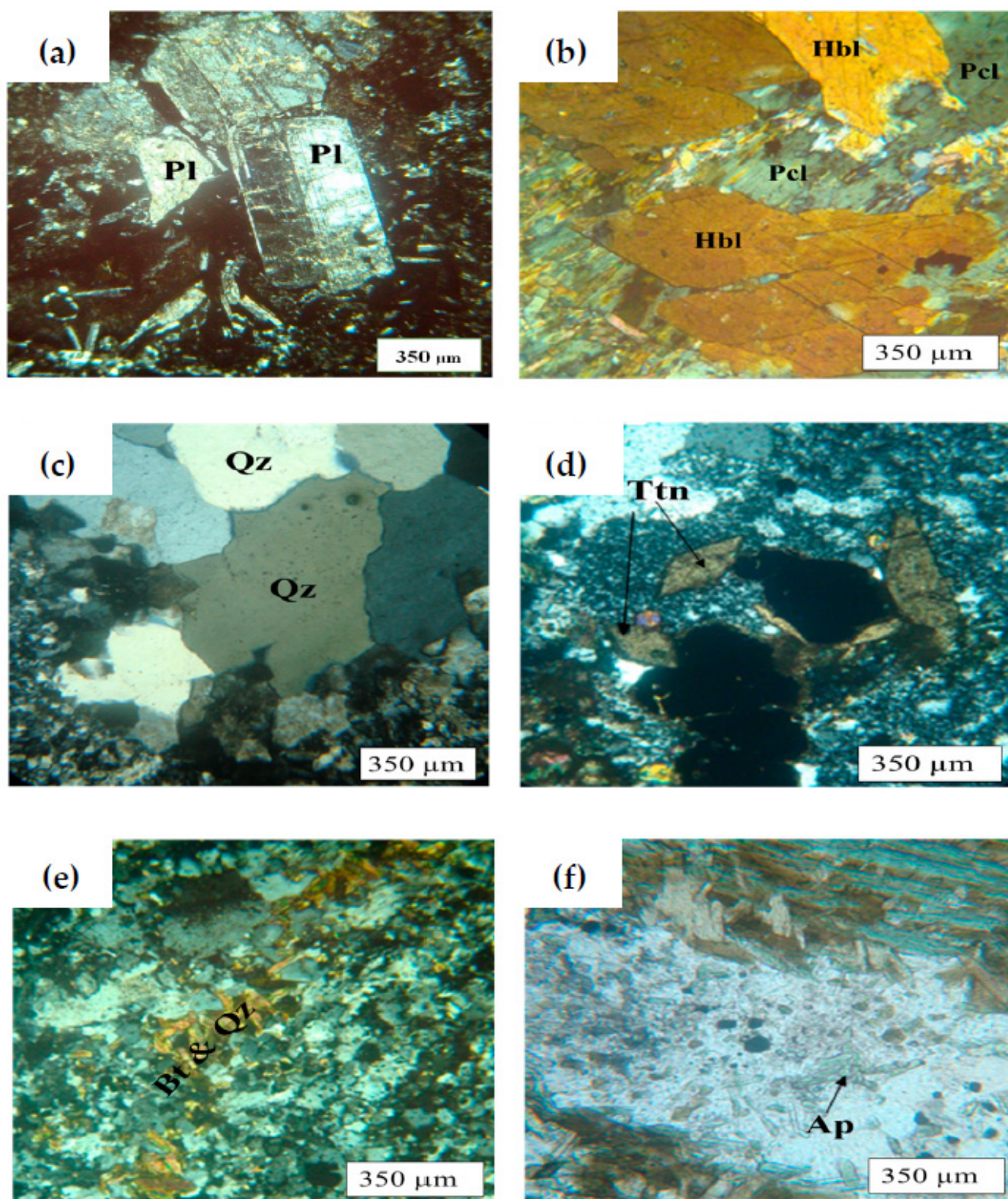


**Figure 5.** (a–f) Photomicrographs showing the main petrographic features of intermediate Dokhan volcanics (mineral abbreviations taken from [25]): (a) tabular prismatic plagioclase crystals exhibit Carlsbad lamellar twinning (CN); (b) pyroxene and hornblende appear in corresponding view (CN); (c) secondary quartz grains filling microfractures and vugs (CN); (d) titanite crystals associated with opaque minerals as a clot (CN); (e) biotite and quartz grains take a trellis-like shape (CN); and (f) apatite and biotite minerals exhibited as having a needle-like shape (PPL).



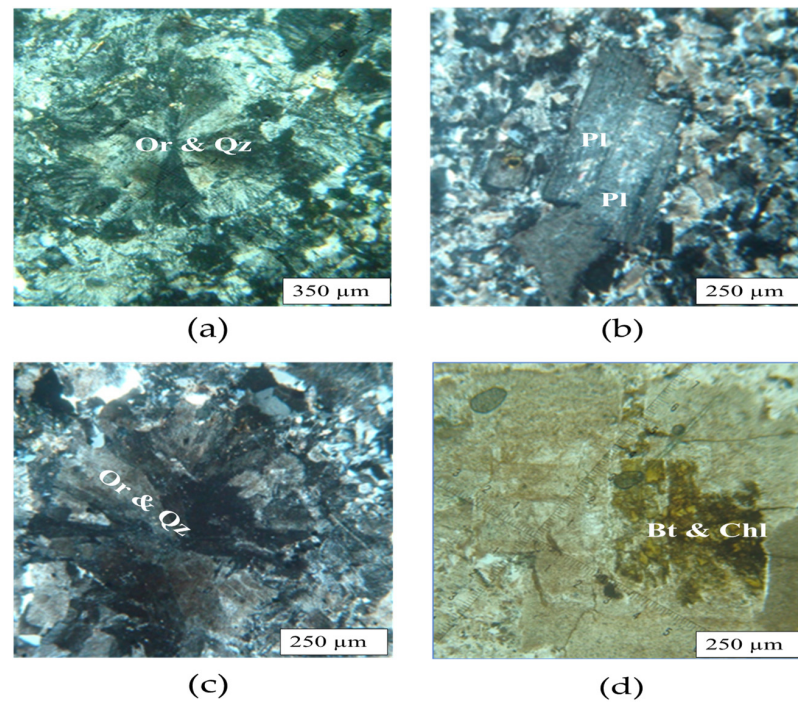


**Figure 6.** (a–d) Photomicrographs showing the main petrographic features of acidic Dokhan volcanics (mineral abbreviations taken from [25]): (a) spherulitic texture (CN); (b) plagioclase crystals exhibit porphyritic texture (CN); (c) fibrous orthoclase and quartz crystals radiating (CN); and (d) biotite and chlorite fine grains scattered on plagioclase minerals (PPL).

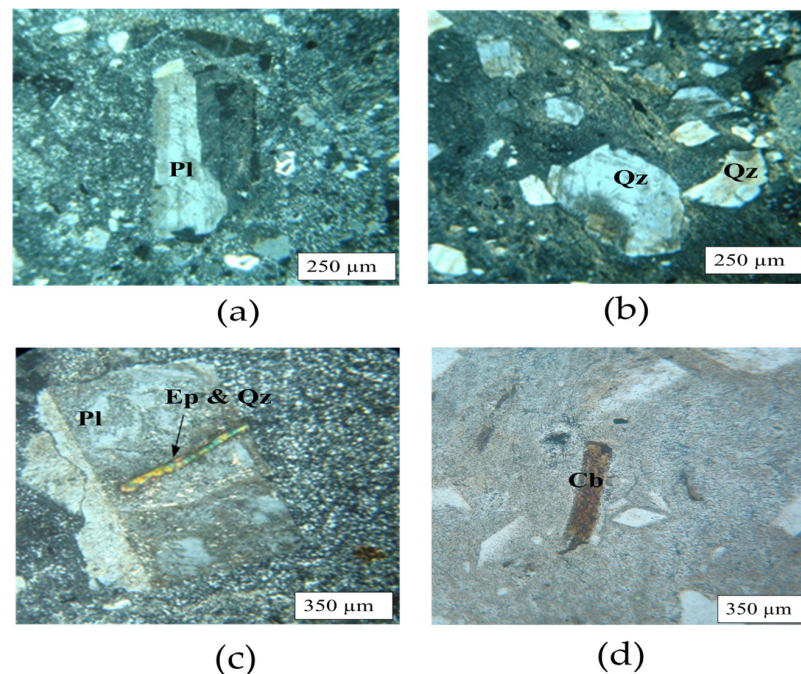


**Figure 7.** (a–d) Photomicrographs showing the main petrographic features of pyroclastic Dokhan volcanics (mineral abbreviations taken from [25]): (a) plagioclase phenocryst set in fine- to medium-grained groundmass of quartz, plagioclase, and iron oxides (CN); (b) rounded to subrounded quartz grains set in cryptocrystalline to glassy groundmass (CN); (c) consolidated ash invaded with phenocrysts of biotite and quartz (CN); and (d) carbonate mineral occurring as secondary minerals filling the microfractures of rock fragments (PPL).

#### 4.2. Geochemistry

In this study, eighteen Dokhan volcanic samples were analyzed for major oxides and trace elements for the purpose of determining their geochemical characteristics (Tables 1–3). Relevant analysis was conducted within the laboratories of the National Research Center of Egypt (NRC). The compositions of Dokhan volcanics exhibit a wide range of silica saturation from basalts to rhyolites (49.65 to 73.21 wt. % SiO<sub>2</sub>) with an average (63.58%) variation. The Harker variation diagrams in Figure 8 display the chemical variations and trends among the related rock varieties. Within such variation diagrams, the plot of SiO<sub>2</sub> against major oxides and trace elements (Figure 8) discriminates two distinct geochemical trends, corresponding to the physicochemical processes that operate in magmatic crystallization. The studied Dokhan volcanics plot of SiO<sub>2</sub> against TiO<sub>2</sub>, Al<sub>2</sub>O<sub>3</sub>, FeO, Fe<sub>2</sub>O<sub>3</sub>, MnO, CaO, P<sub>2</sub>O<sub>5</sub>, Zn, and Sr demonstrate the reversible relationships between SiO<sub>2</sub> and these oxides (Figure 8). Meanwhile, SiO<sub>2</sub> versus Na<sub>2</sub>O, K<sub>2</sub>O, and Rb demonstrate the irreversible relationship(s) between these oxides and SiO<sub>2</sub>.

**Table 1.** Chemical data (major oxides, minor, and trace elements) of the investigated Dokhan volcanics.

Rock Type	Basic Dokhan Volcanics					
	Major Oxides (wt. %)		Trachybasalts			Tholeiitic Basalts
S.No.	1B	2B	5B	1BD	4BD	4US
SiO <sub>2</sub>	56.31	64.64	65.66	57.54	49.65	50.88
TiO <sub>2</sub>	1.55	0.78	0.7	1.18	1.98	1.93
Al <sub>2</sub> O <sub>3</sub>	16.00	16.39	16.9	16.95	16.82	15.71
FeO	4.77	2.28	1.69	4.36	6.95	6.6
Fe <sub>2</sub> O <sub>3</sub>	3.79	2.39	1.91	3.47	4.48	4.62
MnO	0.12	0.09	0.11	0.12	0.19	0.17
MgO	3.74	1.66	1.35	2.27	5.25	5.74
CaO	6.19	3.4	2.71	6.25	5.98	6.23
Na <sub>2</sub> O	3.88	4.28	4.69	2.87	3.17	2.99
K <sub>2</sub> O	2.32	3.5	3.69	3.1	1.99	2.83
P <sub>2</sub> O <sub>5</sub>	0.62	0.26	0.23	0.47	0.89	0.79
SO <sub>3</sub>	0.21	0.08	0.06	0.03	0.08	0.06
Cl	0.03	0.03	0.03	0.03	0.04	0.02
LOI	6.39	0.04	0.71	1.22	1.92	1.09
Total	99.53	99.76	99.73	99.85	99.39	99.64
Trace elements (ppm)						
Zn	145	45	105	0	210	280
Ba	1795	890	870	1110	820	920
Co	150	95	0	130	240	240
Cr	160	0	0	100	0	250
Cu	70	50	0	120	110	100
Ga	0	0	0	40	50	30
Nb	0	0	0	0	10	30
Ni	0	0	0	60	120	170
Pb	0	0	0	30	0	330
Rb	0	0	0	100	60	70
Y	30	35	35	30	30	40
Zr	565	485	560	540	490	540
Sr	1010	500	560	1440	2340	1180
Ce	0	0	0	0	0	0
F	0	0	0	0	620	0
Na <sub>2</sub> O/K <sub>2</sub> O	1.67	1.2	1.27	0.92	1.59	1.05

**Table 2.** Chemical data (major oxides, minor, and trace elements) of the investigated Dokhan volcanics.

Rock Type	Intermediate Dokhan Volcanics					
	Andesite Porphyry		Pyroxene Andesites		Quartz Andesites	Trachytes
Major Oxides (wt. %)	2ID	5ID	7US	10US	16GW	1US
S.No.	2ID	5ID	7US	10US	16GW	1US
SiO <sub>2</sub>	50.70	52.80	55.12	55.34	71.70	59.34
TiO <sub>2</sub>	1.72	1.65	1.38	1.42	0.21	0.98
Al <sub>2</sub> O <sub>3</sub>	18.85	17.61	15.32	14.78	13.93	17.62
FeO	6.07	5.66	4.31	4.65	0.62	2.54
Fe <sub>2</sub> O <sub>3</sub>	4.11	4.53	3.26	3.59	0.90	2.99
MnO	0.15	0.11	0.16	0.12	0.06	0.08
MgO	4.10	3.33	5.54	6.10	0.30	1.69
CaO	5.62	5.06	6.76	6.11	0.96	2.98
Na <sub>2</sub> O	3.40	3.51	3.31	3.01	3.63	5.16
K <sub>2</sub> O	2.08	3.44	2.65	3.05	6.73	4.88
P <sub>2</sub> O <sub>5</sub>	0.71	0.66	0.54	0.56	0.03	0.17
SO <sub>3</sub>	0.15	0.06	0.09	0.17	0.07	0.09
Cl	0.04	0.03	0.04	0.03	0.03	0.02
LOI	1.92	1.52	0.94	0.99	0.46	0.45
Total	99.61	99.97	99.32	99.91	99.28	98.99
Trace elements (ppm)						
Zn	180	140	180	200	0	60
Ba	1600	1650	950	480	420	980
Co	210	270	200	170	0	0
Cr	170	180	290	400	0	0
Cu	0	190	110	60	0	50
Ga	30	40	40	40	20	30
Nb	30	30	0	20	30	0
Ni	140	120	200	220	0	0
Pb	60	80	80	60	30	40
Rb	50	100	60	60	210	100
Y	40	30	30	40	50	30
Zr	730	630	610	590	470	440
Sr	1880	1500	1320	1140	130	980
Ce	0	620	540	640	390	810
F	0	0	1550	0	0	1060
Na <sub>2</sub> O/K <sub>2</sub> O	1.10	1.02	1.25	0.98	0.54	1.05

**Table 3.** Chemical data (major oxide and trace elements) of the investigated Dokhan volcanics.

Rock Type	Acidic Volcanics				Pyroclastics	
	Spherulitic Rhyolites				Agglomerates	
S No.	11GW	15GW	21GW	23GW	13US	26GW
SiO <sub>2</sub>	73.21	66.02	73.20	73.10	68.74	67.26
TiO <sub>2</sub>	0.15	0.80	0.11	0.31	0.4	0.45
Al <sub>2</sub> O <sub>3</sub>	4.19	13.66	14.09	14.15	15.5	16.5
FeO	0.56	2.03	0.46	0.44	1.04	1.01
Fe <sub>2</sub> O <sub>3</sub>	0.78	2.30	0.63	0.63	1.3	1.32
MnO	0.03	0.17	0.02	0.05	0.07	0.08
MgO	0.41	3.21	0.19	0.32	1.1	0.85
CaO	0.72	2.13	0.77	0.66	1.37	1.28
Na <sub>2</sub> O	4.40	4.05	4.46	4.33	4.72	3.16

Table 3. Cont.

Rock Type	Acidic Volcanics				Pyroclastics	
	Spherulitic Rhyolites				Agglomerates	
K <sub>2</sub> O	4.91	4.32	4.63	5.24	4.22	6.17
P <sub>2</sub> O <sub>5</sub>	0.05	0.02	0.03	0.04	0.17	0.12
SO <sub>3</sub>	0.06	0.01	0.04	0.17	0.08	0.03
Cl	0.03	0.03	0.03	0.04	0.02	0.03
LOI	0.40	1.14	0.50	0.47	0.55	0.88
Total	99.91	99.80	99.16	99.93	99.27	99.58
Trace elements (ppm)						
Zn	0	520	0	0	110	80
Ba	720	2700	480	150	1220	1510
Cr	0	220	80	0	60	80
Cu	0	29,420	0	100	40	60
Ga	20	70	30	30	30	30
Nb	20	50	10	20	30	10
Ni	40	80	30	40	40	30
Pb	0	90	30	60	50	60
Rb	160	370	150	160	90	190
Y	40	90	20	50	40	30
Zr	210	1040	200	500	520	470
Sr	150	1010	50	70	560	360
Ce	720	0	190	300	0	0
Na <sub>2</sub> O/K <sub>2</sub> O	0.90	0.94	0.96	0.83	1.12	0.51

According to the variation in K<sub>2</sub>O content with silica, and hence in the Na<sub>2</sub>O/K<sub>2</sub>O ratios, these differences tend to subdivide the silica-saturated alkalic suites into “sodic series” (Na<sub>2</sub>O/K<sub>2</sub>O > 2; e.g., Ascension Island in [26]) and a “potassic series” (Na<sub>2</sub>O/K<sub>2</sub>O < 2; e.g., Nandewar volcano of [27]). In the present study, the (Na<sub>2</sub>O/K<sub>2</sub>O) ratios of all Dokhan volcanic samples that are less than 2 are set in the potassic series. Several discriminatory diagrams were applied to aid in the classification, nomenclature, and interpretation of the tectonic setting of the Dokhan volcanics.

According to the SiO<sub>2</sub> versus Na<sub>2</sub>O + K<sub>2</sub>O binary diagram recommended by the “International Union of Geologist Sciences” (IUGS) for the classification of volcanic rocks, proposed by [28,29], the studied Dokhan volcanics are distributed as trachybasalts, basaltic trachyandesites, trachyandesites, andesites, trachytes, and rhyolites. According to the K<sub>2</sub>O versus SiO<sub>2</sub> chemical classification diagram in [30], the studied Dokhan volcanics mostly fall within the medium- to high-K andesites and dacites. Most samples of these Dokhan volcanics fall within the subalkaline field as per [31], due to its low alkali oxide and silica content compared to the normal ones. Moreover, most samples plotted in the Dokhan volcanics field, suggested by refs. [31,32], used a (Na<sub>2</sub>O + K<sub>2</sub>O)-SiO<sub>2</sub> binary diagram to differentiate between alkaline and subalkaline rocks. According to this diagram, the investigated Dokhan volcanics have a predominantly subalkaline nature.

Meanwhile, five samples within the plot are alkaline due to the increased SiO<sub>2</sub> and Na<sub>2</sub>O + K<sub>2</sub>O. According to the AFM ternary diagram in [31], the geochemical characteristics of the studied Dokhan volcanics are derived from a calc-alkaline magmatic nature. In the Zr-SiO<sub>2</sub> variation diagram in [33,34], the majority of the plotted Dokhan volcanics’ points fall within the active continental margin field, owing to its low Zr value. Meanwhile, the Ni versus FeO/MgO binary diagram in [35] demonstrates the plot of the investigated Dokhan volcanics in the field of island arc and active continental margins (Figure 9).

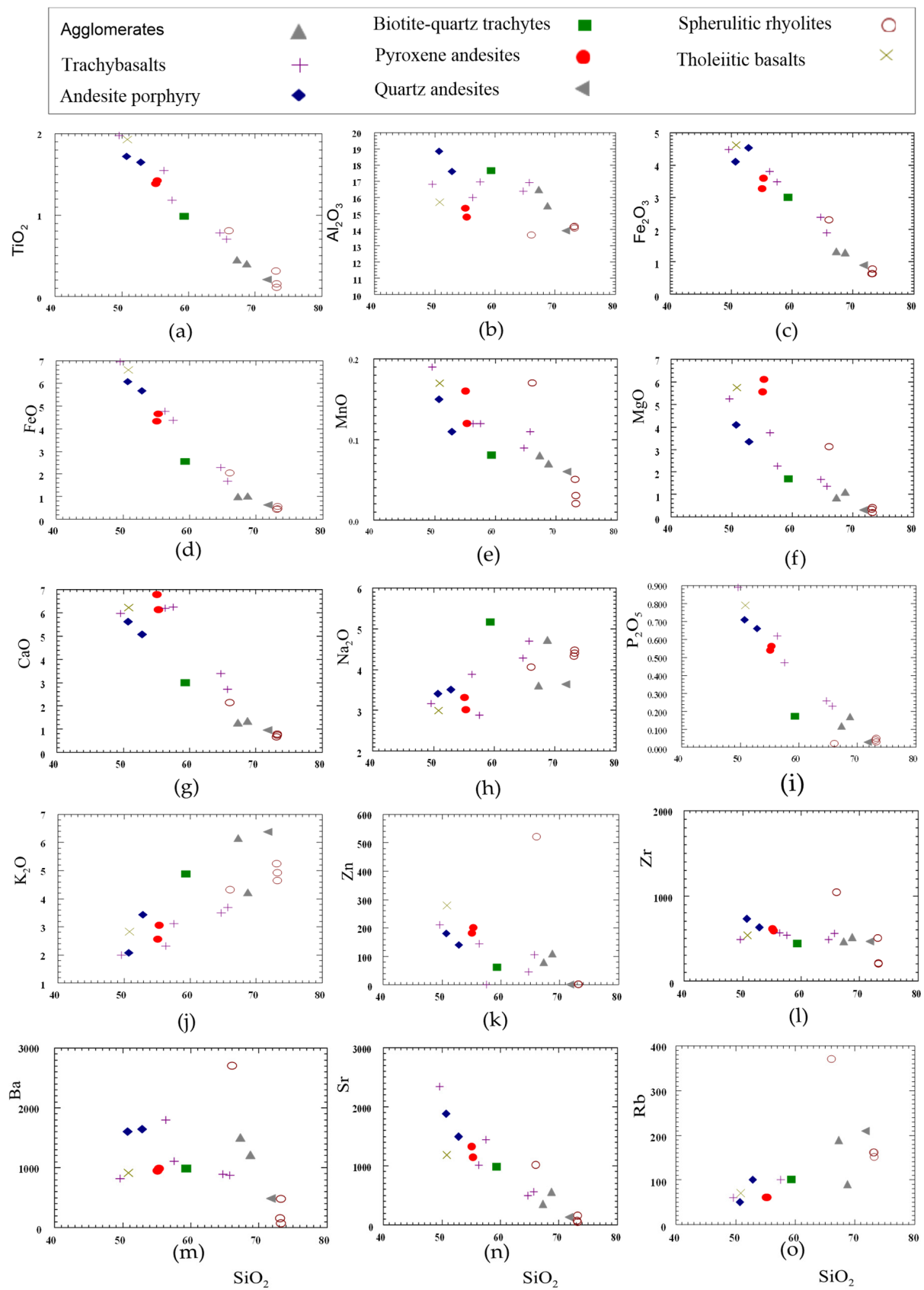
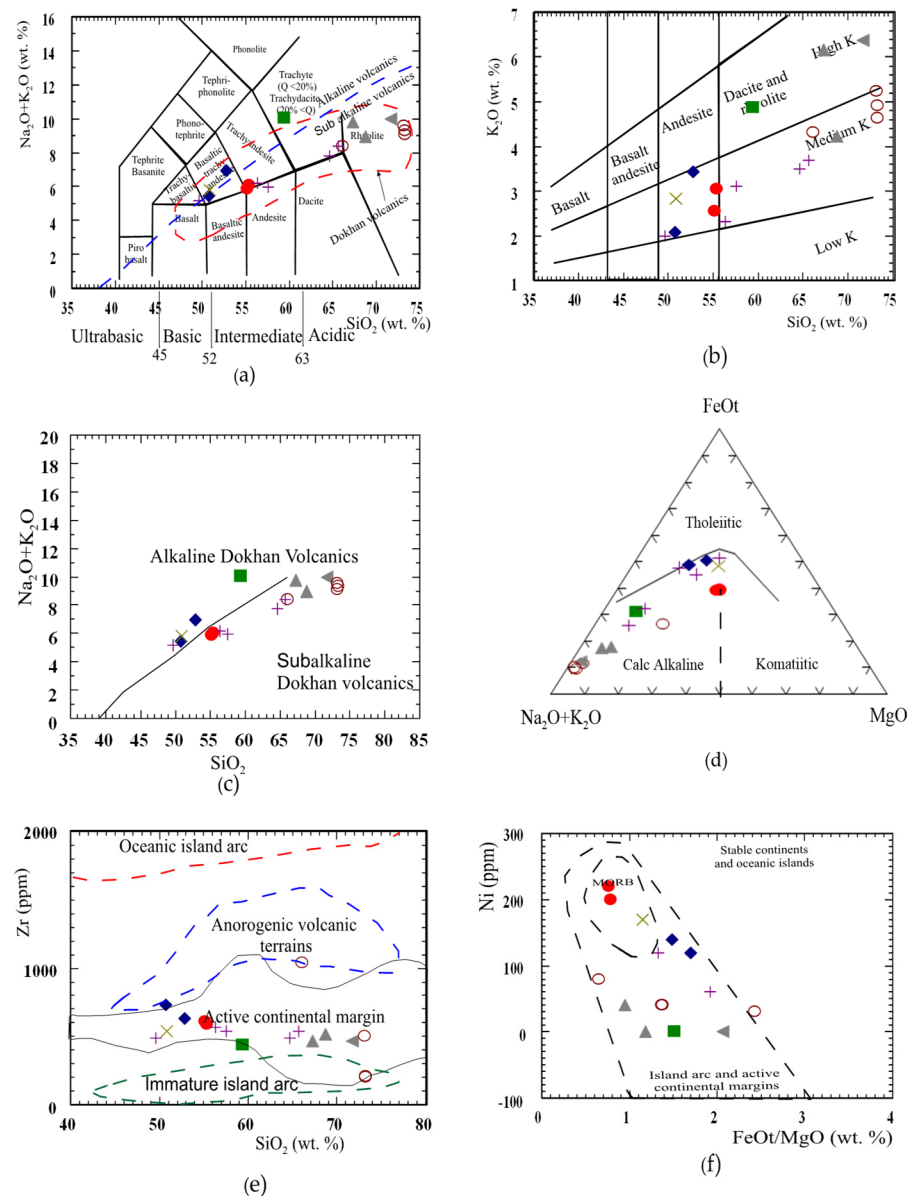


Figure 8. (a–o) Harker’s variation diagrams for the investigated Dokhan volcanics.



**Figure 9.** (a–f) The chemical classification, magma type, and tectonic setting of the investigated Dokhan volcanics (symbols as per Figure 8). (a) Classification and nomenclature of Dokhan volcanics through the total alkali versus silica (TAS) diagram of ref. [28] in ref. [27]. Q = normative quartz; Ol = normative olivine, with the discriminating boundary between alkaline and sub-alkaline fields taken from ref. [31]; field for Dokhan volcanics taken from ref. [32]. (b) K<sub>2</sub>O versus SiO<sub>2</sub> classification diagram for the studied Dokhan volcanics [30]. (c) TAS diagram of the Dokhan volcanics [31]. (d) AFM diagram for the studied Dokhan volcanics showing a distinction between tholeiitic, komatiitic, and calc-alkaline suites [31]. (e) Plots of the Dokhan volcanics on a Zr versus SiO<sub>2</sub> diagram [33,34]. (f) Plots of the Dokhan volcanics on an AFM ternary diagram [35].

#### 4.2.1. Source and Fractionation

Major oxides and trace element variations versus SiO<sub>2</sub> (Figure 8) demonstrate smooth curve trends with gradual decreases in MgO, CaO, Fe<sub>2</sub>O, TiO<sub>2</sub>, P<sub>2</sub>O<sub>5</sub>, and Sr, however, increases with Rb. Meanwhile, some elements such as Al<sub>2</sub>O<sub>3</sub>, Na<sub>2</sub>O + K<sub>2</sub>O, Ba, and Zr illustrate a gradual increase in their contents up to a maximum value of approximately 68 wt. % SiO<sub>2</sub> after which decreases occur with increasing SiO<sub>2</sub> (Figure 10). This feature is common in calc-alkaline igneous suites [36,37], where decreases in Al<sub>2</sub>O<sub>3</sub>, Na<sub>2</sub>O + K<sub>2</sub>O, and Ba can be attributed to the dominant role of feldspar fractionation. The decrease

in Zr is predominantly a result of early crystallization of zircon, due to the decreasing solubility of Zr in a melt with a low alkali/aluminum ratio [38]. Ref. [39] suggested that rhyolites are generally attributed to crustal melting. Ref. [40] indicated that the resistance partial melting for rhyolites and dacites is based primarily on Zr concentrations. Most major oxides and trace element variation diagrams from refs. [40,41] showed trends for trachyandesites that were generally compatible with a model of crystal fractionation in a shallow magma chamber.  $\text{SiO}_2$  saturation is herein increasing with decreases in MgO, FeO, and CaO concentrations, compatible with the crystal fractionation of plagioclase and clinopyroxene. When plotted versus MgO, the concentrations of FeO,  $\text{TiO}_2$ , and  $\text{P}_2\text{O}_5$  initially increase then consequently decrease, indicating the fractionation of Fe-Ti oxides and apatite following the peak (Figure 10).

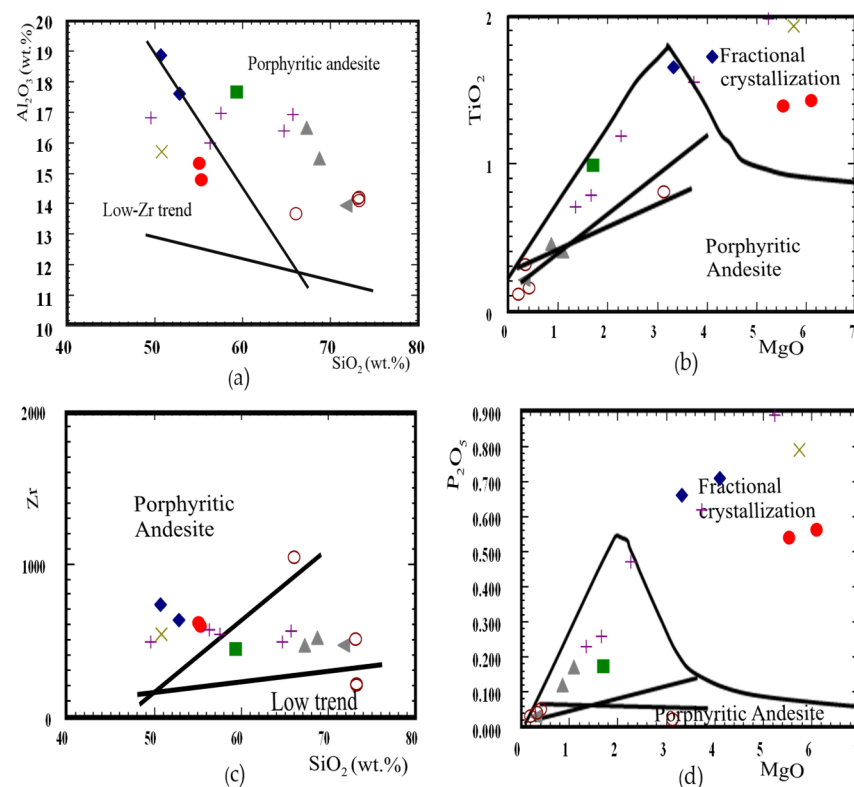


**Figure 10.** (a–d) Variation diagrams showing various trends [40,41]. These trends support crustal fractionation and magma mixing; symbols conform with Figure 8.

Sundry variation diagrams such as in Figure 10 show additional trends that cannot be completely explained by crystal fractionation. Rhyolites plot on a trend of increasing  $\text{SiO}_2$  with decreasing Zr, which indicates late zircon fractionation. As seen in Figure 10d, the concentration of Zr is lower in the more evolved trachyandesites than in the rhyolites. Although most of the trachyandesites seem to follow a trend of fractional crystallization in Figure 10b,c, the rhyolites require a more complex explanation involving both fractional crystallization and magma mixing.

#### 4.2.2. Adakitic Affinity

As originally defined in [42–44], adakites form suites of intermediate to felsic rocks of compositions ranging from hornblende–andesites to dacites and rhyolites with a lack of basaltic members. In these lavas, phenocrysts are mainly zoned plagioclase, hornblende, and biotite whereas orthopyroxene and clinopyroxene phenocrysts are known only in mafic andesites from the Aleutians and Mexico [45–47]. Furthermore, the existing accessory phases are apatite, zircon, titanite, and titanomagnetite. The rocks contain  $\text{SiO}_2 > 56$  wt. %, high  $\text{Na}_2\text{O}$  content ( $3.5 \text{ wt. \%} \leq \text{Na}_2\text{O} \leq 7.5 \text{ wt. \%}$ ), and correlated low  $\text{K}_2\text{O}/\text{Na}_2\text{O}$  ( $\sim 0.42$ ).

Their  $\text{Fe}_2\text{O}_3 + \text{MgO} + \text{MnO} + \text{TiO}_2$  content is moderately high (~7 wt. %), with high Mg (~0.51) and high Ni and Cr content (24 and 36 ppm, respectively). Ref. [40] also reported typically high Sr content (>400 ppm), with extreme concentrations reaching 3000 ppm. As proposed in [42,48], certain geochemical characteristics can be used to discriminate between normal calc-alkaline lavas and adakites. Based on the latter, Dokhan volcanics are divided between adakite and arc magmatic rocks. Fields of delaminated lower crust-derived adakitic rocks and rhyolites are normal calc-alkaline lavas (arc magmatic rocks) of thick lower crust-derived adakitic rocks (Figure 11a,c). The lavas in Dokhan volcanics are pertinent to both the low-silica adakite (LSA) and high-silica adakite (HSA) groups (see Figure 12a–e). Refs. [49,50] identified two distinct adakite groups: high- $\text{SiO}_2$  adakites (rhyolites, HSAs;  $\text{SiO}_2 > 60$  wt. %) and low- $\text{SiO}_2$  adakites (LSAs;  $\text{SiO}_2 < 60$  wt. %). It is generally considered that the reaction with pure slab melts and surrounding peridotites in the sub-arc mantle base results in the high Mg number and MgO content typical of adakites (Figure 11c). The field of metabasalt and eclogite experimental melts (1–4.0 GPa) is in agreement with [51–57]. The field of metabasalt and eclogite experimental melts hybridized with peridotites is as per [52]. The field of subducted oceanic crust-derived adakites was constructed by using data from [42,50,58–64]. Data for the thick lower crust-derived adakitic rocks were obtained from [65–67].

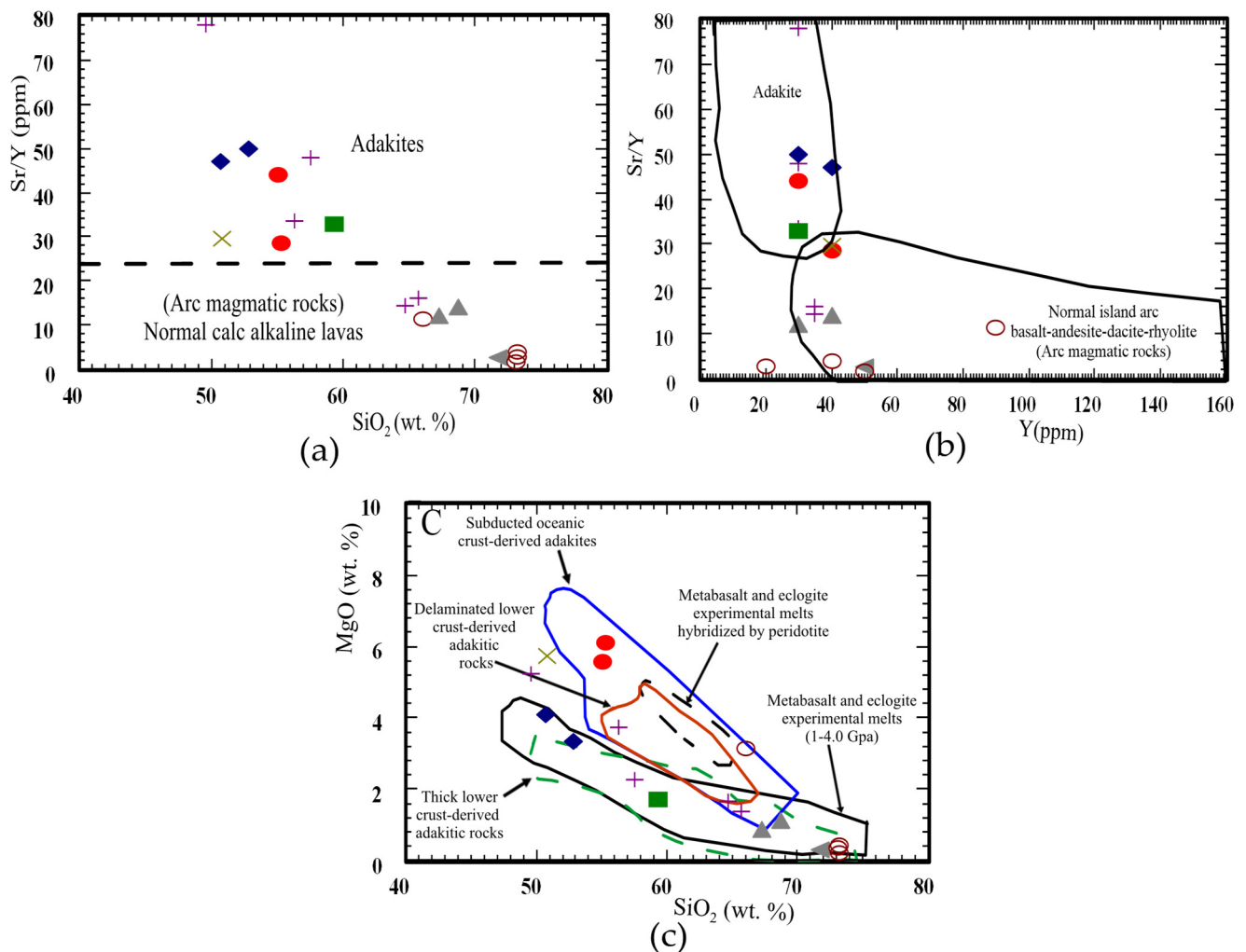


**Figure 11.** (a–c) Binary relations used to differentiate between normal calc-alkaline lavas and adakites: (a)  $\text{SiO}_2$  versus Sr/Y, (b) Y versus Sr/Y as per [42,48], and (c) MgO versus  $\text{SiO}_2$ . Symbols conform with Figure 8.



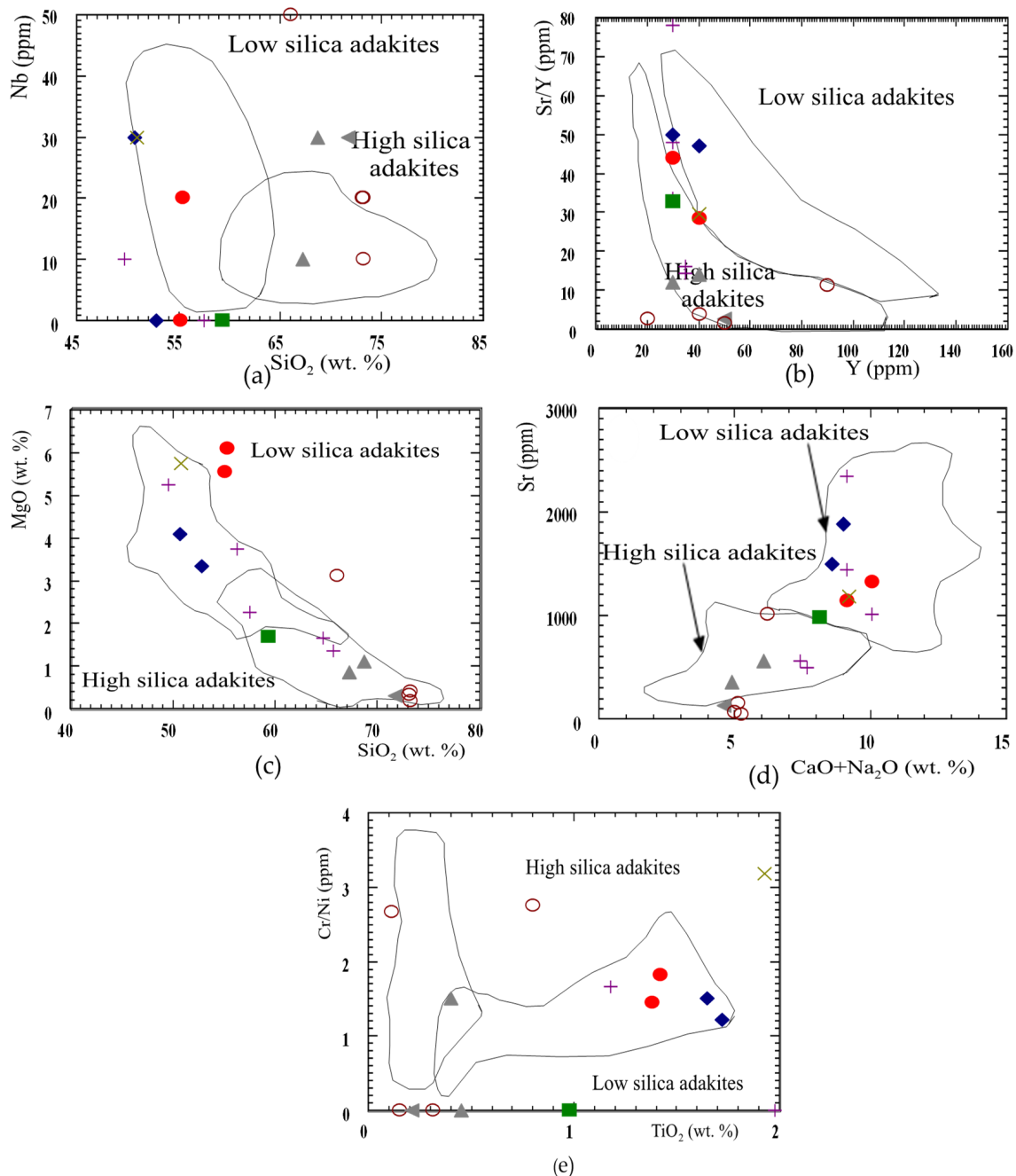


**Figure 12.** (a–e) TiO<sub>2</sub> diagrams comparing high-SiO<sub>2</sub> adakites (HSAs) and low-SiO<sub>2</sub> adakites (LSAs) [49,50] in terms of the following: (a) Nb versus SiO<sub>2</sub>; (b) Sr/Y versus Y; (c) MgO versus SiO<sub>2</sub>; (d) Sr versus (CaO + Na<sub>2</sub>O); and (e) Cr/Ni versus TiO<sub>2</sub>. Symbols conform with Figure 8.

### 4.3. Experimental Procedures

#### 4.3.1. Properties of the Studied Raw Materials

In the current study, conventional concrete was produced by using the following ingredients: (i) Portland cement type I (CEMI 42.5-N), conforming to ASTM C150; (ii) natural sand, whose physical and chemical properties are shown in Tables 4–6; (iii) tap water; and (iv) crushed stone of a maximum nominal size of 25 mm. They were collected from the aforementioned sources (physical and mechanical properties are shown in Tables 7–9, Figures 13 and 14).

**Table 4.** Physical properties of incorporated natural sand.

Property	Test Result	Specification (ES 1109) [68]
Relative density	2.56	N.A
Bulk density (ton/m <sup>3</sup> )	1.53	N.A
Fineness modulus	2.40	3%
Clay and fine material (%)	2.00	≤4.00 (weight)

**Table 5.** Grading of natural sand.

Sieve size (mm)	4.75	2.36	1.18	0.600	0.300	0.150
Passing (%)	99.6	98.6	95.3	85.0	57.6	6.3
Specification (second zone) (ES 1109) [68]	100-89	100-60	100-30	100-15	70-5	15-0

**Table 6.** Chemical analysis of natural sand.

Property	Test Result	Specification (ECP 203) [69]
Chloride (Cl <sup>-</sup> ) content (%)	0.035	≤0.06
Sulfate (SO <sub>3</sub> <sup>-</sup> ) content (%)	0.08	≤0.40

**Table 7.** Specific gravity and water absorption of coarse aggregates.

Sample Location	Wet Density (ton/m <sup>3</sup> )	Apparent Specific Gravity	Bulk Density (ton/m <sup>3</sup> )	Water Absorption %	Specification (ECP 203) [69]
Wadi Abu Zoghot	2.67	2.69	2.66	0.40	≤2.50
Um Sidrah-1Us	2.71	2.73	2.70	0.40	
Um Sidrah-2Us	2.68	2.70	2.68	0.30	
Wadi Al-Ushsh	2.68	2.70	2.67	0.40	
Wadi El-Ghafiryia	2.69	2.70	2.68	0.30	
Wadi Al-Radah-Luman	2.70	2.71	2.69	0.30	
Gabal Ghuwayrib	2.69	2.71	2.68	0.40	
Ataqa (Dolomite)	2.56	2.65	2.51	2.15	

**Table 8.** Sieve analysis for coarse aggregates.

Sieve Size (mm)	Wadi Abu-Zoghot	Om Sidra (1)	Om Sidra (2)	Wadi Al-Ushsh	Wadi Al-Radah- Luman	Wadi El-Ghafiryia	Gabal Ghuwayrib
	Passing (%)						
37.5	100.0	100.0	100.0	100.0	100.0	100.0	100.0
25	95.4	95.6	95.5	95.1	95	96.3	95.9
19	62.6	75.3	62.8	60.8	60	70.6	50.6
12.5	36.0	38.9	35.8	35	41.7	26.4	25.8
9.5	24.0	16.0	22	19.6	28.0	12.2	12.4
4.75	8.0	3.1	7.8	5.2	8.5	5.5	4.4
2.36	2.0	0.4	2.6	0.8	4.3	2	0.9

**Table 9.** Abrasions and impacts using the Los Angeles test.

Sample Location	Rock Type	Los Angeles (%)	Specification (ECP 203) [69]
Wadi Abu Zoghot	Basalt	12.4	≤30%
Um Sidra-1Us	Basalt	11.9	
Um Sidra-2Us	Andesite	14.8	
Wadi Al-Ushsh	Basalt	12.1	
Wadi El-Ghafiryia	Basalt	13.9	
Wadi Al-Radah-Luman	Rhyolite	16.0	
Gabal Ghuwayrib	Mix of Dokhan volcanics	15.1	

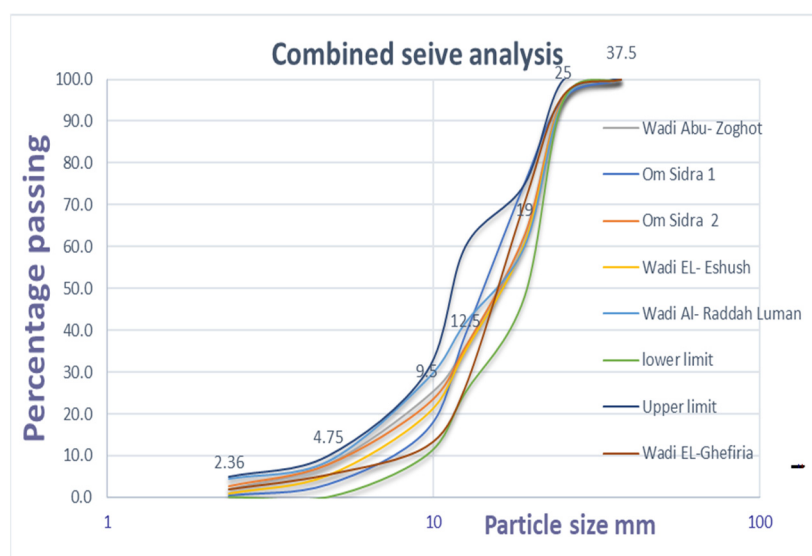


**Figure 13.** Combined chart (sieve analysis) of the Dokhan volcanics’ coarse aggregates.

#### 4.3.2. Mix Design

Herein, the design mix proportions of eight different concrete mixtures, using the aforementioned materials, are presented (see Table 10).

**Table 10.** Concrete mix designs for the study of Dokhan volcanics.

Sample Location	Mix Proportions (per 1 m <sup>3</sup> )						Admixture Type G	Water/Cement Ratio
	Cement	Sand	Agg. 1	Agg. 2	Free Water	Total Water		
Wadi Abu Zoghot	400	626	500	755	160	165	6	41%
Um Sidrah-1Us	400	700	472	707	160	170	6	42.5%
Um Sidra-2Us	400	700	472	707	160	165	6	41%
Wadi Al-Ushsh	400	700	472	707	160	165	6	41%
Wadi El-Ghafiryia	400	700	472	707	160	165	6	41%
Wadi Al-Radah-Luman	400	700	472	707	160	165	6	41%
Gabal Ghuwayrib	400	626	500	755	160	165	6	41%
Ataqa (Dolomite)	400	700	472	707	165	185	7.5	46%

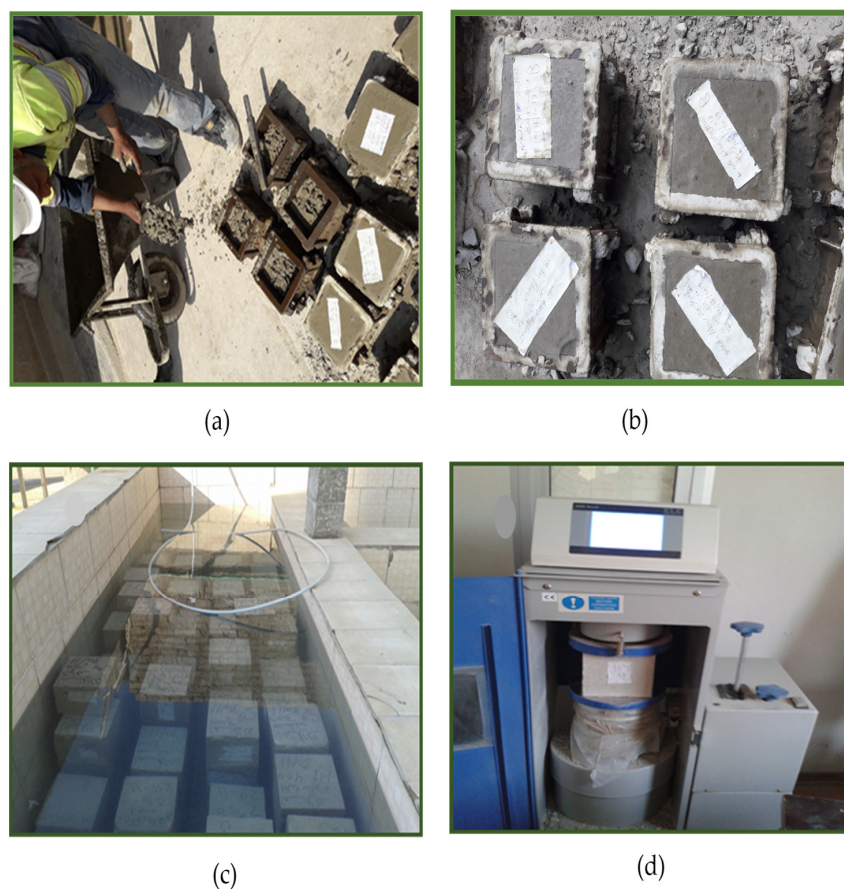


**Figure 14.** (a–d) Stages and methods for the preparation of concrete cubes and their testing according to the specifications of standards.

Three mix proportions were prepared to achieve concrete batches of various strengths. Concrete compressive strength was determined in accordance with ASTM C 39M–03 [30] by casting  $150 \times 300$  mm cylinders. Table 1 elaborates upon the mix proportions and associated concrete compressive strengths.

#### 4.3.3. Concrete Test Results

Fresh concrete results wherein Dokhan volcanics are used as concrete aggregates are presented in Table 11, below.

**Table 11.** Results of fresh concrete Dokhan volcanics.

Sample Location	Initial		After 30 Min		After 60 Min	
	Slump (cm)	Temperature (°C)	Slump (cm)	Temperature (°C)	Slump (cm)	Temperature (°C)
Wadi Abu Zoghot	22	20	21	20	20	20.5
Um Sidra-1Us	20	21.5	19	21.6	18	22
Um Sidra-2Us	22	2.7	21	21	20	21.5
Wadi El-Shush	22	21	20	21.5	19	22
Wadi El-Ghafiryia	22	21	21	21.5	20	22
Wadi Al-Radah Luman	22	21	21	21.5	20	22
Gabal Ghuwayrib	24	19.8	22	20	21	20
Ataqa (Crushed Dolomite)	22	23	19	25	16	26.5

The corresponding hardened concrete results are displayed in Table 12.

**Table 12.** Compressive strength tests of the concrete after 7, 28, and 56 days.

Sample Location	Compressive Strength (MPa)		
	7-Day Age	28-Day Age	56-Day Age
Wadi Abu Zoghot	56.3	67.5	69.6
Um Sidra -1US	39.0	46.8	51.3
Um Sidra -2US	54.8	57.4	65.7
Wadi Al-Shush	49.7	53.7	59.7
Wadi El-Ghafiryia	42.0	50.5	52.5
Wadi Al- Radah -Luman	44.2	48.5	53.0
Gabal Ghuwayrib	51.7	58.5	62.0
Ataqa (Dolomite)	31.0	40.0	41.5

### 5. Discussion

Noting that all concrete mixes, herein, consist of a mixture of sand, crushing dolomite, cement, water, and additives, the reaction of cement begins with mixing and increases with time. When concrete is tested at the age of seven days, the cement paste is of a lesser integrity than dolomite, allowing crack propagation through cement paste. At 28 days, the paste accumulates with time by more than 90% of the required strength, leading to a higher stress capacity for the latter. Consequently, fracture takes place in the dolomite granules instead. It was witnessed that at higher stress levels, the use of crushed Dokhan volcanic rocks in the concrete mixture yielded a significantly higher stress capacity compared to dolomite concrete (see Figure 15).

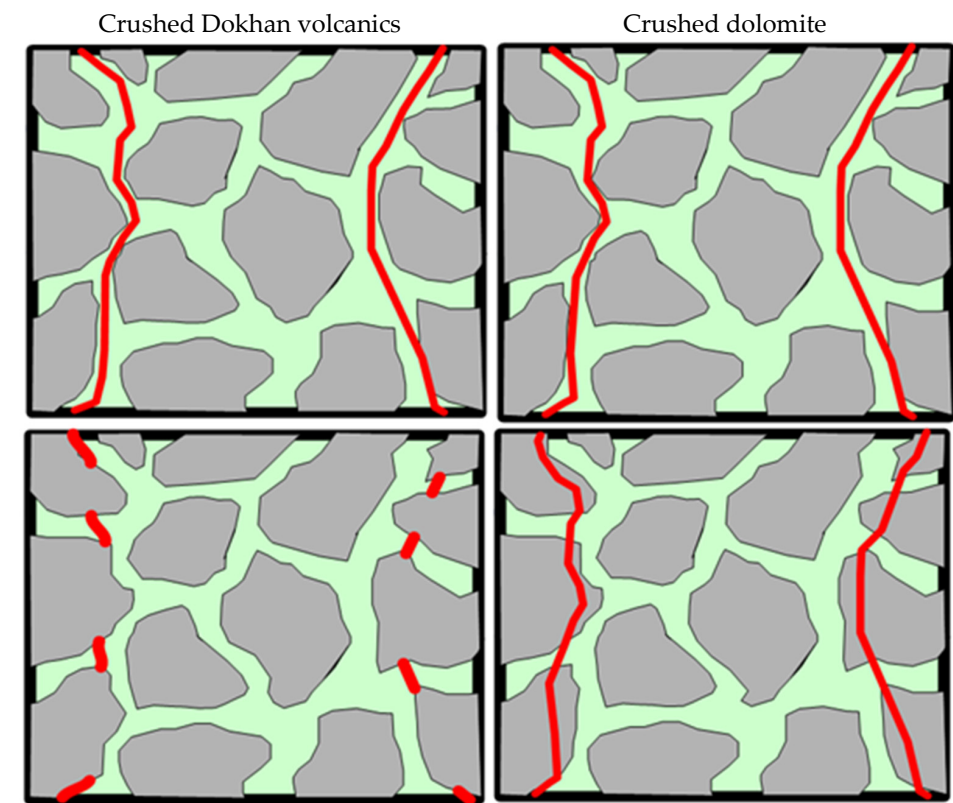


**Figure 15.** The effect of crushed Dokhan volcanics concrete at the ages of 7 and 28 days.

## 6. Conclusions

The present study comprises a wide variety of aggregate(s)/rock from basic, intermediate, and acidic Dokhan volcanics with some pyroclastic rocks. Dokhan volcanics are represented by basalts, andesites, dacites, rhyodacites, rhyolites, and their pyroclastics. Microscopically, these rocks can be identified as trachybasalts, tholeiitic basalts, basaltic andesites, andesites, trachyandesites, dacites, rhyodacites, and spherulitic rhyolites. The composition of Dokhan volcanics in the present study comprises a wide range of silica saturation from basalt to rhyolite (49.65 to 73.21 wt. % SiO<sub>2</sub>) with an average (61.41%) variation. These rocks differ from an alkaline to subalkaline magmatic nature. The geochemical characteristics of calc-alkaline rocks refer to island arcs and active continental margins as well as volcanic rocks of abyssal tholeiite. The study findings also demonstrated as follows:

1. Dokhan volcanics are a suitable alternative that addresses the problem of quarry closures in the Gabal Ataqa area.
2. The tested Dokhan volcanics demonstrate a hardness and corrosion resistance superior to crushed dolomite. The compressive strength of concrete incorporating Dokhan volcanics is higher than that of crushed dolomite, in turn reflected in the concrete's durability.
3. Water absorption for Dokhan volcanics is less than that of crushed dolomite, in turn positively affecting the water-to-cement ratio (w/c) and compressive strength. Consequently, overall cost reduction is anticipated, through the lower cement requirement per cubic meter.
4. Related to using Dokhan volcanics as concrete aggregate—for a cement content of 400 kg/m<sup>3</sup>—these volcanic rocks yield higher compressive strength results after 28 days compared to the corresponding compressive strength of dolomite aggregate. The lowest and highest compressive test results were 46.8 MPa and 67.5 MPa, respectively, yielding an average advantage of 36%, compared to dolomite concrete.

**Author Contributions:** Writing—original draft, A.A.; Writing—review & editing, M.G.H. and T.Y.; Supervision, H.E.-D., N.A.E.-H. and A.K. All authors have read and agreed to the published version of the manuscript.

**Funding:** This research received no external funding.

**Conflicts of Interest:** The authors declare no conflict of interest.

## References

1. Ismail, A.I.M.; Sadek, G. Acidic rocks as Aggregates in Concrete: Engineering Properties, Microstructures and Petrologic Characteristics. *Geotech. Geol. Eng.* **2009**, *27*, 519–528. [[CrossRef](#)]
2. El-Desoky, H.M.; Ahmed, E.K. Petrography and Geochemistry of Basic Dokhan Volcanics from the Eastern Desert of Egypt and their use as Aggregates in Concrete Mixes. *Arab. J. Geosci.* **2015**, *8*, 6791–6809. [[CrossRef](#)]
3. Kishore, I.S.; Mounika, L.; Prasad, C.M.; Krishna, B.H. Experimental Study on the use of Basalt Aggregate in Concrete Mixes. *Int. J. Civ. Eng.* **2015**, *2*, 39–42.
4. Al-Zou'by, J.; Al-Zboon, K.K. Effect of Volcanic Tuff on the Characteristics of Cement Mortar. *Cerâmica* **2014**, *60*, 279–284. [[CrossRef](#)]
5. Medeiros, S.I.F.; João, N. Identification of Alkali-Silica Reactions in Santa Maria Island Airport. In Proceedings of the International Multidisciplinary Scientific GeoConference (SGEM), Albena, Bulgaria, 17–26 June 2014; Volume 2, pp. 487–494.
6. Ozbek, A.M.U.; Aydin, D. Estimating Uniaxial Compressive Strength of Rocks Using Genetic Expression Programming. *J. Rock Mech. Geotech. Eng.* **2013**, *5*, 325–329. [[CrossRef](#)]
7. Mathew, E.M.; Jamal, S.M.; Abraham, R. Weathered Crystalline Rock: Suitability as Fine Aggregate in Concrete—A Comparative Study. *Int. J. Innov. Res. Sci. Eng. Technol.* **2013**, *2*, 960–969.
8. Aydin, A.C.; Karakoç, M.B.; Düzgün, O.A.; Bayraktutan, M.S. Effect of Low-Quality Aggregates on the Mechanical Properties of Lightweight Concrete. *Sci. Res. Essays* **2010**, *5*, 1133–1140.
9. Yasar, E.; Tolgay, A.; Teymen, A. Industrial Usage of Nevşehir-Kayseri (Turkey) Tuff stone. *World Appl. Sci. J.* **2009**, *7*, 271–284.
10. De Gennaro, R.; Cappelletti, P.; Cerri, G.; De'Gennaro, M.; Dondi, M.; Graziano, S.F.; Langella, A. Campanian Ignimbrite as Raw Material for Lightweight Aggregates. *Appl. Clay Sci.* **2007**, *37*, 115–126. [[CrossRef](#)]

11. Kabesh, M.L.; Shahin, A.N. Geology of the Basement Rocks of Esh El Mellaha Range. *Desert Inst. Bull.* **1969**, *2*, 109–149.
12. Kabesh, M.L.; Abdel Khaleek, M.Z.; Refaat, A.M. Geology of Wadi El Mellaha Range, Eastern Desert (UAR). *J. Geol.* **1970**, *14*, 53–84.
13. Abu El-Leil, I.; Khalaf, I.M.; Sweifi, B.; Heikal, M.A. The Dokhan volcanics of Esh El Mellaha Range, Petrography, Tectonic Environment and Petrogenesis. *Al-Azhar Bull. Sci.* **1990**, *1*, 69–80.
14. El Sheshtawi, Y.A.; El Tokhi, M.M.; Ahmed, A.M. Petrogenesis of the Dokhan Volcanics of Wadi Dib and Wadi Abu Had, Esh El Mellaha, North Eastern Desert, Egypt. *Ann. Geol. Surv. Egypt* **1997**, *20*, 163–184.
15. El-Rahmany, M.M. Petrography and Petrochemistry of some Dokhan volcanics, Eastern Desert, Egypt (Wassif Volcanics). Master's Thesis, Faculty of Science, Al-Azhar University, Cairo, Egypt, 1979.
16. Moghazi, A.M. Geochemistry and Petrogenesis of a High-K Calc-Alkaline Dokhan Volcanic Suite, South Safaga Area, Egypt: The Role of Late Neoproterozoic Crustal Extension. *Precambrian Res.* **2003**, *125*, 161–178. [[CrossRef](#)]
17. Asran, A.M.H. Geochemistry and Petrogenesis of Neoproterozoic Nuqara Dokhan Volcanics, Central Eastern Desert, Egypt. *Fac. Sci. Bull. (Assiut Univ.)* **2003**, *32*, 69–88.
18. Gharib, M.E.; Ahmed, H.A. Late Neoproterozoic Volcanics and Associated Granitoids at Wadi Ranga, South Eastern Desert, Egypt: A Transition from Subduction Related to Intra-Arc Magmatism. *Lithos* **2012**, *155*, 236–255. [[CrossRef](#)]
19. Khalaf, E.E.D.A.H. Origin and Evolution of Post-Collisional Volcanism: An Example from Neoproterozoic Dokhan Volcanics at Gabal Nugara Area, Northeastern Desert, Egypt. *Arab. J. Geosci.* **2012**, *5*, 663–695. [[CrossRef](#)]
20. Yaseen, I.A.A.B.; Abidrabbu, A.Y. Mineralogy, Petrology and Geochemistry of the Basalt Flows at Ash-Shun Ash-Shamaliyya Area, North West Jordan. *Earth* **2016**, *5*, 82–95.
21. Khalil, A.E.; El-Desoky, H.M.; Shahin, T.M.; Abdelwahab, W. Late Cryogenian Arc-Related Volcaniclastic Metasediment Successions at Wadi Hammuda, Central Eastern Desert, Egypt: Geology and Geochemistry. *Arab. J. Geosci.* **2018**, *11*, 74. [[CrossRef](#)]
22. EL Desoky, H.M.; Shahin, T.M. Characteristics of Lava-Sediments Interactions During Emplacement of Mid-Tertiary Volcanism, Northeastern Desert, Egypt: Field Geology and Geochemistry Approach. *Arab. J. Geosci.* **2020**, *13*, 328. [[CrossRef](#)]
23. Schmid, R. Descriptive Nomenclature and Classification of Pyroclastic Deposits and Fragments. *Geol. Rundsch.* **1981**, *70*, 794–799. [[CrossRef](#)]
24. Egyptian Mineral Resources Authority. *Geologic Map of Hurghada (AL-Ghardaqa) Quadrangle, Scale 1:250,000*; Egyptian Mineral Resources Authority: Cairo, Egypt, 2005.
25. Whitney, D.L.; Evans, B.W. Abbreviations for Names of Rock-Forming Minerals. *Am. Mineral.* **2010**, *95*, 185–187. [[CrossRef](#)]
26. Harris, C. The petrology of Lavas and Associated Plutonic Inclusions of Ascension Island. *J. Petrol.* **1983**, *24*, 424–470. [[CrossRef](#)]
27. Stolz, A.J. The role of Fractional Crystallization in the Evolution of the Nandewar Volcano, North-Eastern New South Wales, Australia. *J. Petrol.* **1985**, *26*, 1002–1026. [[CrossRef](#)]
28. Bas, M.L.; Maitre, R.L.; Streckeisen, A.; Zanettin, B. A chemical Classification of Volcanic Rocks Based on the Total Alkali-Silica Diagram. *J. Petrol.* **1986**, *27*, 745–750. [[CrossRef](#)]
29. Mario, E.T. *Classification of Igneous Rocks and Glossary of Terms*; Recommendations of the IUGS Subcommittee on the Systematics of Igneous rocks; Blackwell Scientific Publications: London, UK, 1980; p. 34.
30. Le Maitre, R.W. *Igneous Rocks: A Classification Glossary of Terms*, 2nd ed.; Cambridge University Press: New York, NY, USA, 2002; p. 237.
31. Irvine, T.N.; Baragar, W.R.A. A Guide to the Chemical Classification of the Common Volcanic Rocks. *Can. J. Earth Sci.* **1971**, *8*, 523–548. [[CrossRef](#)]
32. Eliwa, H.A.; Kimura, J.; Itaya, T. Late Neoproterozoic Dokhan Volcanics, North Eastern Desert, Egypt: Geochemistry and Petrogenesis. *Precambrian Res.* **2006**, *151*, 31–52. [[CrossRef](#)]
33. Ewart, A. A Review of the Mineralogy and Chemistry of Tertiary-Recent Dacitic, Latitic, Rhyolitic, and Related Salic Volcanic Rocks. *Dev. Petrol.* **1979**, *6*, 13–121.
34. Ewart, A. *The Mineralogy and Petrology of Tertiary-Recent Orogenic Volcanic Rocks*; with Special Reference to the Andesitic-Basaltic Compositional Range; John Wiley: London, UK, 1982; pp. 25–87.
35. Miyashiro, A.; Shido, F. Tholeiitic and Calc-Alkaline Series in Relation to the Behavior of Titanium, Vanadium, Chromium and Nickle. *Am. J. Sci.* **1975**, *275*, 265–277. [[CrossRef](#)]
36. Miller, C.F.; Mittlefehldt, D.W. Extreme Fractionation in Felsic Magma Chambers: A Product of Liquid-State Diffusion or Fractional Crystallization. *Earth Planet. Sci. Lett.* **1984**, *68*, 151–158. [[CrossRef](#)]
37. Abdel-Rahman, A.F.M. Pan-African Volcanism: Petrology and Geochemistry of the Dokhan Volcanic Suite in the Northern Nubian Shield. *Geol. Mag.* **1996**, *133*, 17–31. [[CrossRef](#)]
38. Watson, E.B. Zircon Saturation in Felsic Liquids: Experimental Results and Applications to Trace Element Geochemistry. *Contrib. Mineral. Petrol.* **1979**, *70*, 407–419. [[CrossRef](#)]
39. Tronnes, R.G. *Geology and Geodynamics of Iceland: Unpublished Field Guide (Internal Document)*; University of Iceland: Reykjavik, Iceland, 2002; pp. 22–30.
40. Meganck, A. Stratigraphy and Petrology of Volcanics from an Abandoned Tertiary Rift in Langadalsfjall, Iceland. In Proceedings of the Seventeenth Annual Keck Research Symposium in Geology Proceedings, Washington and Lee University, Lexington, VA, USA, 1 April 2004; pp. 135–138.

41. Defant, M.J.; Drummond, M.S. Derivation of Some Modern Arc Magmas by Melting of Young Subducted Lithosphere. *Nature* **1990**, *347*, 662–665. [[CrossRef](#)]
42. Maury, R.C.; Sajona, F.G.; Pubellier, M.; Bellon, H.; Defant, M.J. Fusion de la Croûte Océanique dans les Zones de Subduction/Collision Récentes: L'exemple de Mindanao (Philippines). *Bull. Soc. Geol. Fr.* **1996**, *167*, 579–595.
43. Martin, H. Adakitic Magmas: Modern Analogues of Archean Granitoids. *Lithos* **1999**, *26*, 411–429. [[CrossRef](#)]
44. Kay, R.W. Aleutian Magnesian Andesites: Melts from Subducted Pacific Ocean Crust. *J. Volcanol. Geotherm. Res.* **1978**, *4*, 117–132. [[CrossRef](#)]
45. Rogers, G.; Saunders, A.D.; Terrell, D.J.; Verma, S.P.; Marriner, G.F. Geochemistry of Holocene Volcanic Rocks Associated with Ridge Subduction in Baja California, Mexico. *Nature* **1985**, *315*, 389–392. [[CrossRef](#)]
46. Calmus, T.; Aguillón-Robles, A.; Maury, R.C.; Bellon, H.; Benoit, M.; Cotten, J.; Bourgois, J.; Michaud, F. Spatial and Temporal Evolution of Basalts and Magnesian Andesites (“Bajaites”) from Baja California, Mexico: The Role of Slab Melts. *Lithos* **2003**, *66*, 77–105. [[CrossRef](#)]
47. Defant, M.J.; Drummond, M.S.; Mount, S. Helens: Potential Example of the Partial Melting of the Subducted Lithosphere in a Volcanic Arc. *Geology* **1993**, *21*, 547–550. [[CrossRef](#)]
48. Martin, H.M.; Moya, J.F.M. Secular Changes in TTG Composition: Comparison with Modern Adakites. In Proceedings of the EGS-AGU-EUG Joint Assembly, Nice, France, 6–11 April 2003; pp. 26–73.
49. Martin, H.; Smithies, R.H.; Rapp, R.; Moya, J.F.; Champion, D. An Overview of Adakite, Tonalite–Trondhjemite–Granodiorite (TTG) and Sanukitoid: Relationships and Some Implications for Crustal Evolution. *Lithos* **2005**, *79*, 1–24. [[CrossRef](#)]
50. Rapp, R.P.; Watson, E.B.; Miller, C.F. Partial Melting of Amphibolite/Eclogite and the Origin of Archean Trondhjemites and Tonalites. *Precambrian Res.* **1991**, *51*, 1–25. [[CrossRef](#)]
51. Rapp, R.P.; Shimizu, N.; Norman, M.D.; Applegate, G.S. Reaction between Slab-Derived Melts and Peridotite in the Mantle Wedge: Experimental Constraints at 3.8 GPa. *Chem. Geol.* **1999**, *160*, 335–356. [[CrossRef](#)]
52. Rapp, R.P.; Xiao, L.; Shimizu, N. Experimental Constraints on the Origin of Potassium-Rich Adakite in East China. *Acta Petrol. Sin.* **2002**, *18*, 293–311.
53. Sen, C.; Dunn, T. Experimental Modal Metasomatism of a Spinel Iherzolite and the Production of Amphibole-Bearing Peridotite. *Contrib. Mineral. Petrol.* **1994**, *119*, 422–432. [[CrossRef](#)]
54. Rapp, R.P.; Robert, P.; Bruce, W.E. Dehydration Melting of Metabasalt at 8–32 kBar: Implications for Continental Growth and Crust-Mantle Recycling. *J. Petrol.* **1995**, *36*, 891–931. [[CrossRef](#)]
55. Prouteau, G.; Scaillet, B.; Pichavant, M.; Maury, R.C. Fluid-Present Melting of Ocean Crust in Subduction Zones. *Geology* **1999**, *27*, 1111–1114. [[CrossRef](#)]
56. Skjerlie, K.P.; Patiñodouce, A.E. The fluid-absent partial melting of a zoisite-bearing quartz eclogite from 1.0 to 3.2 GPa; Implications for melting in thickened continental crust and for subduction-zone processes. *J. Petrol.* **2002**, *43*, 291–314. [[CrossRef](#)]
57. Kay, R.W.; Kay, S.M. Delamination and Delamination Magmatism. *Tectonophysics* **1993**, *219*, 177–189. [[CrossRef](#)]
58. Drummond, M.S.; Defant, M.J.; Kepezhinskas, P.K. Petrogenesis of Slab-Derived Trondhjemite–Tonalite–Dacite/Adakite Magmas. *Earth Environ. Sci. Trans. R. Soc. Edinb.* **1996**, *87*, 205–215.
59. Stern, C.R.; Kilian, R. Role of the Subducted Slab, Mantle Wedge and Continental Crust in the Generation of Adakites from the Andean Austral Volcanic Zone. *Contrib. Mineral. Petrol.* **1996**, *123*, 263–281. [[CrossRef](#)]
60. Sajona, F.G.; Maury, R.C.; Pubellier, M.; Leterrier, J.; Bellon, H.; Cotton, J. Magmatic Source Enrichment by Slab-Derived Melts in a Young Post-Collision Setting, Central Mindanao (Philippines). *Lithos* **2000**, *54*, 173–206. [[CrossRef](#)]
61. Aguillón, R.A.; Calmus, T.; Benoit, M.; Bellon, H.; Maury, R.C.; Cotten, J.; Michaud, F. Late Miocene Adakites and Nb-Enriched Basalts from Vizcaino Peninsula, Mexico: Indicators of East Pacific Rise Subduction Below Southern Baja California. *Geology* **2001**, *29*, 531–534. [[CrossRef](#)]
62. Defant, M.J.; Kepezhinskas, P.; Defant, M.J.; Xu, J.F.; Kepezhinskas, P.; Wang, Q.; Xiao, L. Adakites: Some Variations on a Theme. *Acta Petrol. Sin.* **2002**, *18*, 129–142.
63. Atherton, M.P.; Petford, N. Generation of Sodium-Rich Magmas from Newly Underplated Basaltic Crust. *Nature* **1993**, *362*, 144–146. [[CrossRef](#)]
64. Muir, R.J.; Weaver, S.D.; Bradshaw, J.D.; Eby, G.N.; Evans, J.A. The Cretaceous Separation Point Batholith, New Zealand: Granitoid Magmas Formed by Melting of Mafic Lithosphere. *J. Geol. Soc.* **1995**, *152*, 689–701. [[CrossRef](#)]
65. Petford, N.; Atherton, M. Na-Rich Partial Melts from Newly Underplated Basaltic Crust: The Cordillera Blanca Batholith, Peru. *J. Petrol.* **1996**, *37*, 1491–1521. [[CrossRef](#)]
66. Johnson, K.; Barnes, C.G.; Miller Christopher, A. Petrology, Geochemistry, and Genesis of High-Al Tonalite and Trondhjemites of the Cornucopia Stock, Blue Mountains, Northeastern Oregon. *J. Petrol.* **1997**, *38*, 1585–1611. [[CrossRef](#)]
67. Xiong, X.L.; Li, X.H.; Xu, J.F.; Li, W.X.; Zhao, Z.H.; Wang, Q.; Chen, X.M. Extremely High-Na Adakite-Like Magmas Derived from Alkali-Rich Basaltic Underplate: The Late Cretaceous Zhantang Andesites in the Huichang Basin, SE China. *Geochem. J.* **2003**, *37*, 233–252. [[CrossRef](#)]



- 
68. *Egyptian Standards ES 1109 (Aggregates for Concrete)*; Egyptian Organization for Standards and Quality: Cairo, Egypt, 2021; p. 52.
  69. National Housing and Building Research Center (HBRC). *Egyptian Code of Practice ECP 203*, 5th ed.; National Housing and Building Research Center (HBRC): Giza, Egypt, 2020; pp. 21–26.

**Disclaimer/Publisher's Note:** The statements, opinions and data contained in all publications are solely those of the individual author(s) and contributor(s) and not of MDPI and/or the editor(s). MDPI and/or the editor(s) disclaim responsibility for any injury to people or property resulting from any ideas, methods, instructions or products referred to in the content.